Electronic Journal of Structural Engineering

Original Article

Cite this: DOI:10.56748/ejse.26930

Received Date: 28 November 2025
Accepted Date: 8 January 2026

1443-9255
https://ejsei.com/ejse

Ground deformation of site with an exciting fault-crossing tunnel and deformation evaluation on tunnel subjected to normal faulting

Zhiyong Liu [a], Lingyin Zhao [a], Dan Zhang [a], Cheng Gong [a], Ping Geng[b, c*], Tianqiang Wang [b, c]

[a] Chengdu Engineering Corporation Limited, Chengdu, Sichuan 610072, China
[b] State Key Laboratory of Intelligent Geotechnics and Tunnelling, Southwest Jiaotong University, Chengdu, Sichuan, 610031, China
[c] School of Civil Engineering, Southwest Jiaotong University, Chengdu 610031, China
*Corresponding author: 13551258484@139.com

Abstract

Fault-crossing tunnels are vulnerable especially when the fault dislocation happens. The fault dislocation affects the deformation on ground surface and failure on underground structures, and it is vital for crossing-fault tunnel to reveal dislocation mechanisms. Thus, based on different fault parameters such as width of fault fracture zone and fault dip, three experimental tests were carried out to obtain the ground deformation and failure of tunnel with a self-designed large-scaled model box. The test results firstly show that the fault parameters affect ground deformation and tunnel structures. Under the fault dislocation effects, four sub-regions were identified on ground surface as stability region in footwall, coordination region, severe deformation region and stability region in hanging wall. The parameter influence from fault fracture zone will be sensitive for tunnel and the tunnel near fault fracture zone is most damaged. Typical damage types can be divided into four categories according to the degree of damage and moderate damage or serious damage should be avoided as far as possible to guarantee the normal operation of the tunnel.

Keywords

Fault-crossing tunnel, Model test, Ground deformation, Fault dislocation, Failure mechanism

1. Introduction

Current studies suggest that co-seismic dislocation of faults is the main cause of earthquakes, and surface movement and permanent deformation caused by fault movement will cause damage to surface and underground buildings in the affected area (Hashimoto et al., 1996). In Wenchuan earthquake, In the 2008 Wenchuan earthquake, both the main fault and the secondary fault produced surface tilt and rupture parallel to the fault strike, resulting in offset or collapse of surface buildings in Beichuan and Yingxiu towns (Zhou et al., 2010), as shown in Figure 1, and dislocation damage of related tunnel projects.

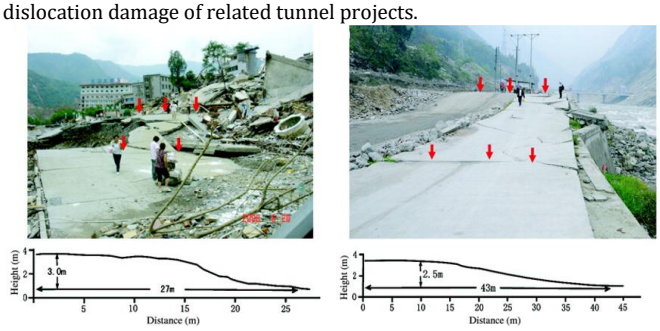

(a) Beichuan County in Wenchuan (b) Yingxiu Town in Wenchuan

Fig. 1 Photos of surface deformation caused by faults (Zhou et al., 2010)

Active fault is an important geological phenomenon related to a series of theoretical problems such as structural geology, seismology and geodynamics. From a technical and economic point of view, the tunnel route will be avoid crossing from the adverse geological zone to ensure the safety of the tunnel during construction and operation (Li et al., 2023; Bao et al., 2023). The development of traffic tunnel engineering, especially long tunnel, is bound to provide the necessary premise for the balanced development of economic construction in various regions of China. However, the route design of long tunnels is sometimes inevitably close to or through active faults. The deformation of overlying soil caused by bedrock fault dislocation will inevitably cause catastrophic and irreversible damage to ground surface and underground structures (Scholz et al., 2019).

The study of ground deformation features and tunnel damage is very important for engineering safety. The statistical analysis method was used to study the width of surface deformation caused by different types of active faults and concluded that the width of active fault avoidance zone was 30 m (Xu et al., 2007). Dai et al. (2008) studied the effects of critical fault displacement and critical sedimentary layer thickness on the fracture propagation characteristics of strike-slip faults and reverse faults through simulation experiments. Bo et al. (2019) and Shen et al. (2022) studied the surface deformation under the reverse fault dislocation by centrifuge test and then predicted the surface rupture by logistic regression analysis.

For understanding of tunnel deformation and failure under bedrock dislocation, scholars have carried out a lot of research works on the influence of fault dislocation on tunnel. Lin et al. (2007) studied deformation mechanism and structural safety of tunnel through model test. Wang et al. (2016) and Han et al. (2021) studied the deformation and failure of tunnels under fault dislocation through model tests and numerical analysis respectively. The influence of fault fracture zone and structure mechanical response were investigated. Kiani et al. (2016) carried out a series of model tests on the problem of dislocation of shallow buried tunnels under normal faulting, and analyzed the phenomenon caused by surface soil collapse. Liu et al. (2015) simulated the failure characteristics of tunnel structures under the stick-slip dislocation of normal faults with dip angles of 60°, 65° and 70° through indoor sand box tests, and explored the interaction of stratum and structure.

Although the deformation and failure on ground surface and tunnel structures caused by fault dislocation have been studied, most studies on the surface failures are based on specific events. The conclusions are usually qualitative based on experience and disaster appearance. There is a lack of in-depth study on the characteristics of surface deformation, so that it is impossible to quantitatively reveal uniform soil deformation and failure under normal faulting, especially at the site with fault fracture zone. In addition, the dislocation response of the cross-fault tunnel structure has a certain relationship with the fault parameters, that is, the change of the fault parameters will lead to different dislocation deformation and failure degree of the tunnel structure. Thus, the deformation failure mechanism of faulting-crossing tunnel considering different fault parameters under normal faulting, and the convergence deformation of lining still needs to be studied. Thus, three sets of large-scaled normal faulting dislocation model tests were designed and implemented here to analysis the ground deformation and tunnel deformation and failure mode. The research results can provide a reference for the prediction of the ground deformation under different faulting magnitudes and a theoretical reference for the anti-fault design for fault-crossing tunnels.

2. Model test

2.1 Apparatus for the test

The test adopted self-designed large scale steel frame structure model box. A self-designed model box for this test is manufactured specially, as shown in Figure 2. The length, width and height of this model box, as shown in Figure 2 are 3.0 m, 1.5 m and 1.5 m respectively. For observation, a welded steel framework form is used around the box. Four pieces of transparent plexiglass are bonded on the framework structure tightly. Steel plate of the model box is divided into two parts, one for moving part, the other for fixed part. The two parts represent hanging wall and foot wall respectively. An angle-adjustable and speed-controlled hydraulic jack is mounted below the steel plate of hanging wall. The jack can automatically exert an imposed displacement with a low velocity of 0.01mm/s to simulate faulting dislocation. In the model test, to simulate normal fault dislocation, a preset uplift on hanging wall is reserved for jack retracting. Furthermore, vinyl was laid on dislocation-induced plate gap to prevent soil leakage during the experiment.

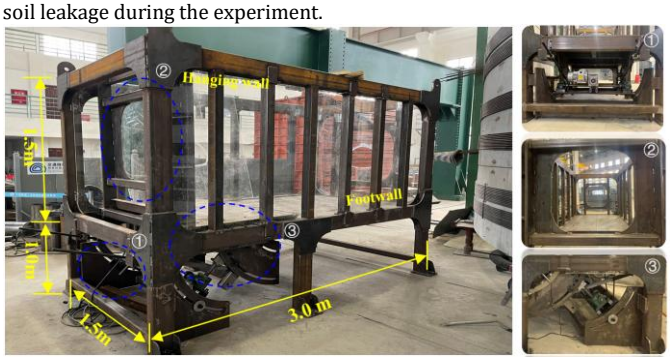

Fig. 2 Apparatus for model test

2.2 Similarity materials and ratio

The geometric similarity ratio of this model test is set to 1: 40 according to the model box size and site conditions. According to the similarity theory, the geometric similarity ratio (C_l=0.025), the unit weight similarity ratio (C_γ=0.8) and the elastic modulus similarity ratio (C_E=0.025) are taken as the basic similarity ratios of model test. The similarity ratios of other physical parameters are calculated according to Bockingham π theorem. The physical parameters involved in the model test and the theoretical similarity of each parameter are shown in Table 1.

Table 1. Test similarity ratios

Parameters	Similarity parameters	Dimension	Designed similarity ratio
Length (l)	C_l	L	1/40
Elastic modulus (E)	C_E	FT^2L^{-4}	1/40
Density (ρ)	C_ρ	FL^{-2}	1/1.25
Poisson's ratio (μ)	C_μ	–	1/1
Strain (ε)	C_ε	–	1/1
Cohesion (c)	$C_c=C_EC_\varepsilon$	FL^{-2}	1/40
Friction (φ)	C_φ	–	1/1

The material for tunnel model uses gypsum with brittle characteristics, which is very similar to the characteristics of quasi-brittle concrete materials. In order to select similar materials that can better reflect the lining and surrounding rock, multiple sets of material tests were carried out before the test to determine the mix ratio of lining, surrounding rock and fracture zone, so as to ensure the accurate simulation of the model test. After the preparation of multiple sets of samples and the determination of uniaxial compression and direct shear tests, the final test material similarity ratio was determined. The main determination process and photographs are shown in Figure 3 In the model test studied in this paper, the materials needed in the model test are first determined according to the material test. Subsequently, the tunnel structure model was determined and produced, and maintenance was carried out. When the curing strength is appropriate, the filling work is carried out. When the model soil is filled to the tunnel position, the tunnel is assembled, and the compactness of the soil is tested for each layer of soil.

In the model test studied in this paper, the materials needed in the model test are first determined according to the material test. Subsequently, the tunnel structure model was determined and produced, and maintenance was carried out. When the curing strength is appropriate, the filling work is carried out. When the model soil is filled to the tunnel position, the tunnel is assembled, and the compactness of the soil is tested for each layer of soil. When the tunnel model soil is filled to the top of the model box, the model is allowed to stand for one day and then the displacement meter is installed, and the dislocation test is carried out.

The final mix ratio of lining material is water, gypsum and diatomite =1: 0.7: 0.2, in which diatomite is mainly used to adjust weight and elastic modulus of mixture. Surrounding rock material is mainly river sand, the test added waste oil to provide the cohesion of the mixture. The final mix ratio is fly ash, river sand, oil and diatomite = 1: 0.74: 0.25: 0.47. The mix proportion of fault fracture zone is fly ash: river sand: oil: sawdust: fly ash = 1: 0.74: 0.25: 0.2: 0.47. The physical and mechanical parameters in the prototype and model tests of surrounding rock, fault fracture zone and lining are listed in Table 2.

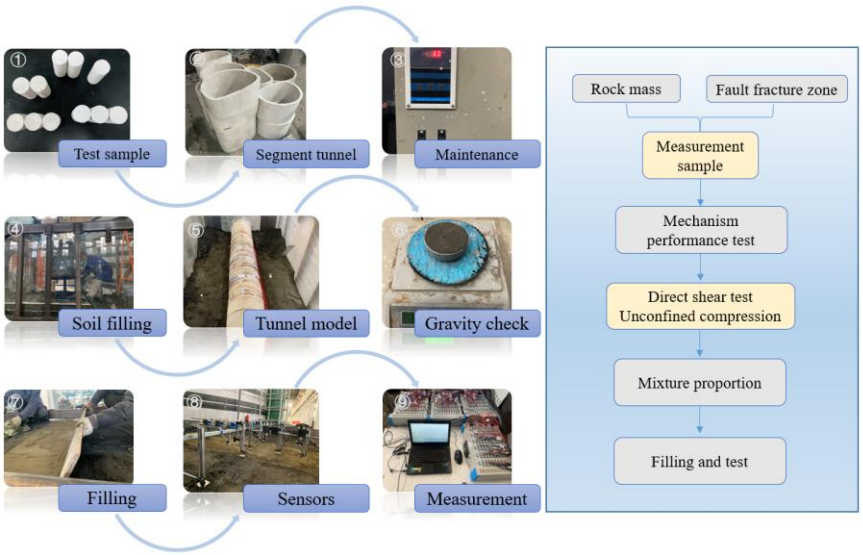

Fig. 3 The main fault dislocation test process

Table 2. Mechanical parameters of materials

Object	Item	Density (kg/m³)	Elastic modulus (MPa)	Poisson's ratio	Cohesion (kPa)	Friction (°)
Surrounding rock	Prototype	2000	2,000	-	200	27
	Model	1620	50	-	4.9	26.8
Ratio	-	1.23	40	-	40.8	1.0
Fault fracture zone	Prototype	1700	900	-	150	22
	Model	1370	22.4	-	3.69	21.3
Ratio	-	1.24	40.2	-	40.7	1.0
tunnel linings	Prototype	2400	30,000	0.25	-	-
	Model	1920	750	0.24	-	-
Ratio	-	1.25	40.0	1.0	-	-

Table 3. Test cases information

Cases	Fault dip /°	Fault width /cm
1	55	40
2	65	50
3	70	50

In the tests, the segmental tunnels with 15cm are set near the fault fracture zone to accurately simulate the lining of the prototype tunnel segment of 6m. The length of tunnel lining segments closed to and away from the fault fracture zone was set to 22 cm and 30 cm respectively. In order to consider the reinforcement of the prototype tunnel, the diameter and spacing of the steel wire mesh for the model are considered as 0.5mm and 0.5cm respectively. Before the test, the hanging wall needs to be lifted to the highest point by jack, so as to reserve enough dislocation space.

In the test, the configured model soil needs to be layered into the model box. Soil compaction needs to be done to ensure accurate simulation of surrounding rock strength. During the filling process, a white quartz sand line is set per 10 cm to measure fault rupture. When the filling height reaches the pre-set height of tunnel, the tunnel model is installed, and then soil is filled with constantly checking the density of soil. When the filling height reaches the top of the model box, stop filling. In order to meet the tectonic stress level required by the model test, the tunnel model maintains statically for one day. Table 3 shows the test cases. The dip angles of three common normal faults in the range of 60° ~90 ° were selected in the test, which were set to 55°, 65° and 70° respectively. Fault fracture zone width is set to 40cm and 50cm.

2.3 Measurement

In the model test, multiple linear differential displacement meters were used to monitor the settlement displacement of the soil surface and the vertical relative displacement of the tunnel, and multi-channel acquisition instruments were used to collect the data. In the study, nine surface displacement meters were set up along the surface center line, named DZ1 ~ DZ9. The nine longitudinal displacement meters are arranged according to the following rules: DZ3 and DZ4 are arranged at the junction of the surface fault zone and the surrounding rock, DZ7 is arranged directly above the bottom between the two plates, and the remaining measuring points are evenly arranged according to the distance. To measure the absolute and relative displacement of tunnel, vertical displacement sensors were installed in the tunnel model. A total of 15 sections were set up in the tunnel, and an in-tunnel displacement meter was set up in 6 sections E, G, H, J, L and N to monitor the displacement of the top and bottom of the tunnel structure. The layout of surface displacement points for measurement is shown in Figure 4.

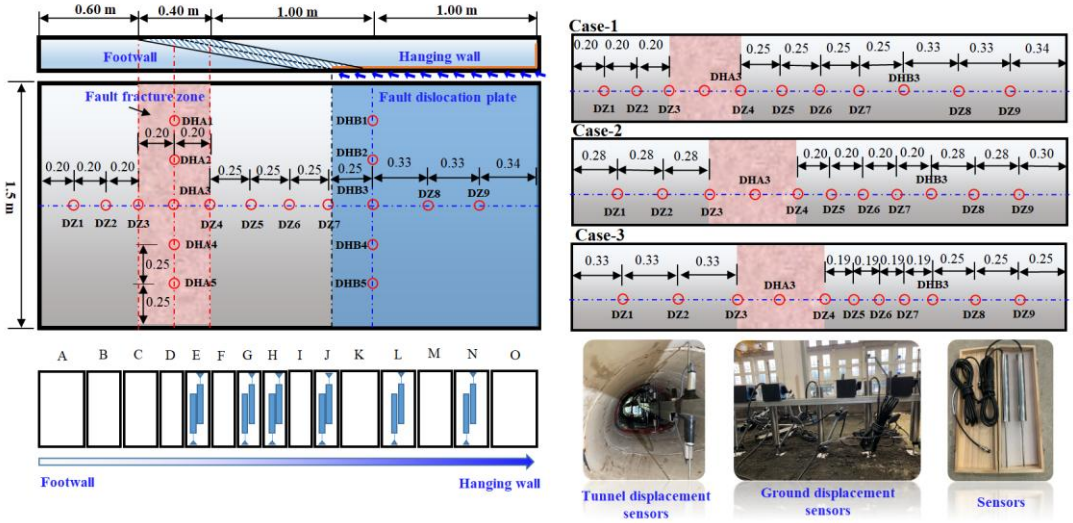

Fig. 4 Displacement measurement points on ground surface and tunnel

3. Test results

3.1 Ground deformation features

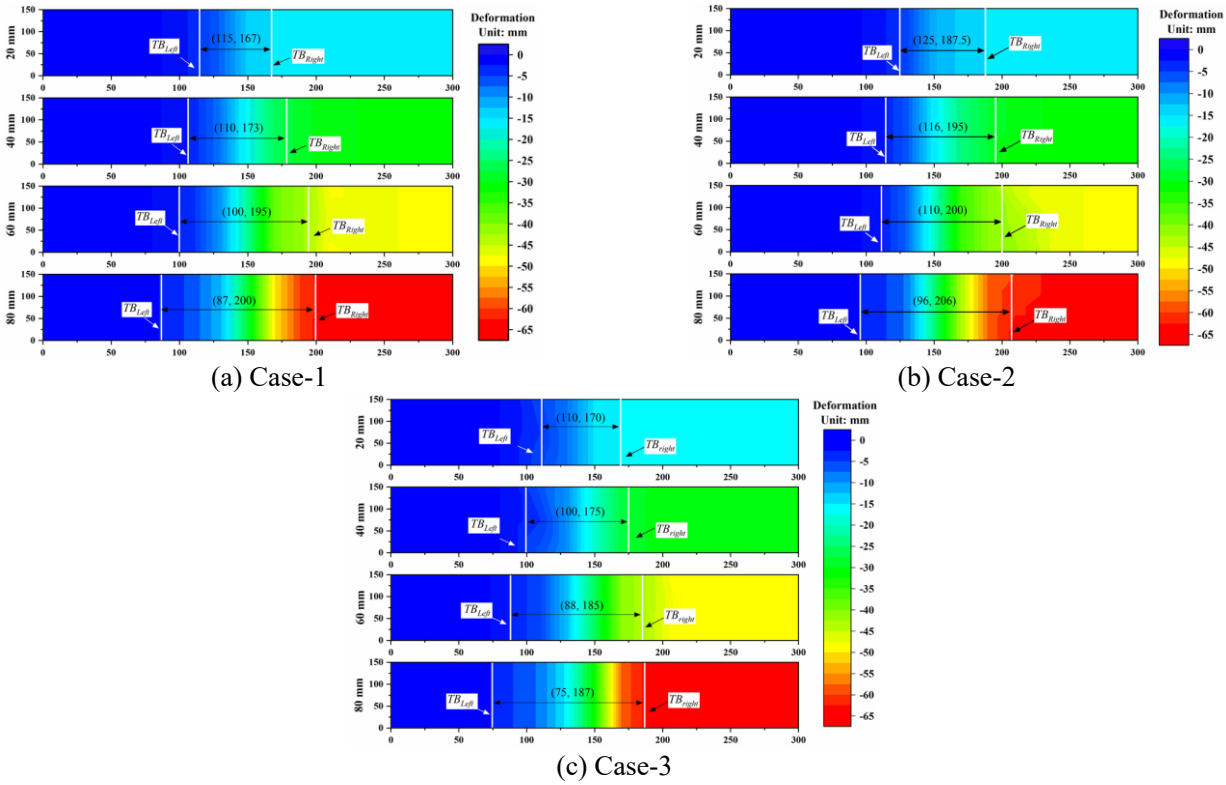

(a) Case-1 (b) Case-2

(c) Case-3

Fig. 5 Ground deformation contours of three cases along longitudinal tunnel

Figure 5 shows the settlement deformation cloud diagram of the surface under different dislocations in three working conditions. According to the surface deformation cloud map under various working conditions, the displacement consistent zone at both ends and the displacement transition zone in the middle can be identified. For convenience, both sides of the displacement transition zone are named as left transition boundary (TB_{Left}) and right transition boundary (TB_{Right}).

Obviously, the range of displacement transition zones is greatly affected by the dislocation. With the gradual increase of dislocation, the range of transition zones also increases. In addition, the range of transition zones with wide fracture zone is larger than that with narrow fracture zones assuming that the boundary of the tunnel near the foot wall is the origin of the coordinate and it is positive along the longitudinal direction of the tunnel. In the Case-1, In the model with a fault dip angle of 55 ° and a fault fracture zone width of 40 cm, when the dislocation momentum is 20 mm, the interval between the point where the surface fixed plate does not produce displacement and the point where the surface in the active plate does not produce uneven settlement along the longitudinal direction is 115 cm to 167 cm. In the model with a fault dip angle of 65 ° and a fault fracture zone width of 50 cm, the interval between the points where the surface fixed plate does not produce displacement and the points where the surface in the active plate does not produce uneven settlement along the longitudinal direction is 125 cm to 187.5 cm when the dislocation is 20 mm. In the model with a fault dip angle of 70 ° and a fault fracture zone width of 50 cm, the interval between the points where the surface fixed plate does not produce displacement and the points where the surface in the active plate does not produce uneven settlement along the longitudinal direction is 110 cm to 170 cm when the dislocation is 20 mm.

The surface transition zones of Case-1 and Case-2 under the initial 20 mm are (115~167) and (125~187.5), respectively. The corresponding transition zone widths are 52 cm and 62.5 cm, respectively, which are about 1.3 times and 1.25 times of the corresponding bandwidth. However, compared with Case-2, the surface transition zone of working Case-3 under small dislocation degree (20mm) is slightly smaller, with a value of 60 cm and a decrease of about 4%. However, when the bedrock dislocation reaches 60 mm, the surface transition zone with narrow width will increase more than the range under the previous dislocation level (40 mm), from 63 cm to 95 cm. Combined with the propagation of surface rupture, this is due to the fact that the fault fracture under the narrow band deviates from the propagation direction along the fault fracture zone, and the fan-shaped fault rupture trajectory will be formed. When the loading continues, the fracture propagates to the ground, which is not on fault. The surface transition zone under small dislocation will be easily affected by the fault width.

According to the ground deformation obtained from the cloud map, the deformation of the ground surface along the longitudinal direction of the tunnel is fitted. Further, in order to characterize the surface displacement of the ground from the fixed plate to the moving plate, Figure 6 shows the ground deformation of the three groups of model tests when the dislocation is 7.5mm, 15mm, 30mm, 45mm and 60mm, and is expressed by logarithmic coordinates. Under different dislocation momentum conditions, there is always an intersection point in surface deformation. The intersection points in the three working conditions appear at 812 mm, 855 mm and 1125 mm, respectively. With the increase of fault dip angle, the position of this intersection gradually moves to the side of the active plate, and the smaller the fault dip angle, the more significant the intersection. When the fault dip angle is large, the intersection is not obvious, which may be related to the surface rupture mode.

3.2 Ground distribution zones

By observing the final deformation characteristics of the surface, the surface deformation changes abruptly in a certain range and tends to be in a non-deformation state away from the fault plane. In view of this, the surface deformation can be divided into four sub-regions: stability region in footwall (R_s in footwall), coordination region (R_c) and severe deformation region (R_{sd}). and Stability region in hanging wall (R_s in hanging wall), as shown in Figure 7 Although the stable area of the hanging wall has declined, as a whole with the dislocation of the bedrock, there is no change in the slope of the surface, and it is still at a general level. The deformation coordination zone is the transition zone between the surface stability zone and the severe deformation zone. The surface within the range has both settlement deformation and slope change, but the degree of deformation is small. The severe deformation zone is the central area affected by the fault dislocation. The surface subsidence in the area is large, and the tilt deformation is severe, which belongs to the range that needs to be paid attention to in the project.

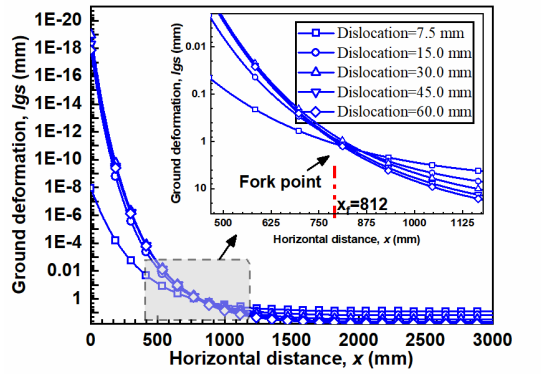

(a) Case-1

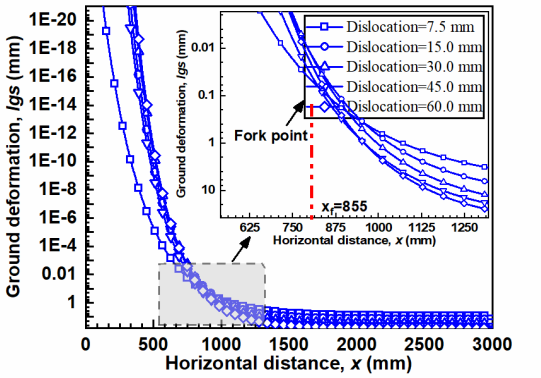

(b) Case-2

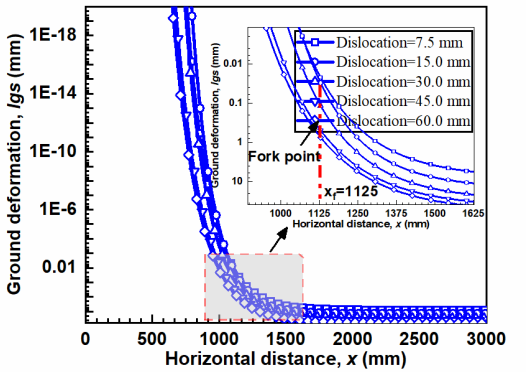

(c) Case-3

Fig. 6 Ground deformation fork point analysis under different fault dislocation

Fig. 7 Diagram of ground deformation distribution zones

According to the research result, the surface rupture caused by the reverse fault can be divided into four stages: the overall uplift period, the uplift deformation period, the scarp translation period and the deformation lag period (Shen et al., 2020). Compared with the reverse fault, there is no obvious hysteresis trend in the process of normal fault dislocation. The surface deformation caused by the normal fault in this paper can be summarized into four stages: (1) The overall subsidence period: when the dislocation momentum is less than 10 mm, the surface of the hanging wall decreases as a whole, but there is no obvious deformation on the surface, and the surface subsidence is less than 8mm; (2) Settlement deformation period: dislocation 10mm-20mm, the fault plane extends, the surface deformation curve appears obvious inflection point, began to occur local deformation; (3) Settlement expansion period: the dislocation momentum is 20mm-50mm, the surface subsidence value of the hanging wall is increasing, and the deformation zone is not significantly increased; (4) Steep inclination increase period: the dislocation momentum is 50 mm~80 mm, the settlement continues to increase, and the steep inclination of the surface near the fault surface increases significantly.

According to the deformation and failure characteristics of the surface, it can be seen that with the gradual increase of the fault dip angle, the surface deformation changes, especially the coordination region (R_c) and severe deformation region (R_{sd}). As the fault dip angle increases, the severe deformation region (R_{sd}) gradually narrows. Coordination region (R_c) did not change significantly

4. Tunnel deformation and failure

4.1 Longitudinal deformation pattern

Affected by fault dislocation, the tunnels are bound to be disturbed and deformed and even damaged. An S-typed longitudinal deformation of tunnel appears. This typical longitudinal profile has been verified in Case-1, as shown in Figure 8 The concentrated severe deformation area produces obvious separation between the segments. The most serious deformation is concentrated on the I, J and K segments in fault fracture zone, in which torsional deformation of the segments and the obvious amount of dislocation between the segments appeared. Under the effect of fault dislocation, these sections with more serious deformation show the displacement transition from the footwall to the concentrated settlement area of hanging wall. A deflection of about 15° from the horizontal direction occurs when the fault dip is small and the width of the fault fracture zone is 40 cm. All these local defections lead to the opening and dislocation between tunnel sections. The deformation mode of the segment of the tunnel structure changes significantly after the change of the fault dip angle of 5 degrees in Case-2 and Case-3, and the overall performance is the deflection of segment K, but the longitudinal direction of the tunnel structure is more uniform when the dip angle is larger.

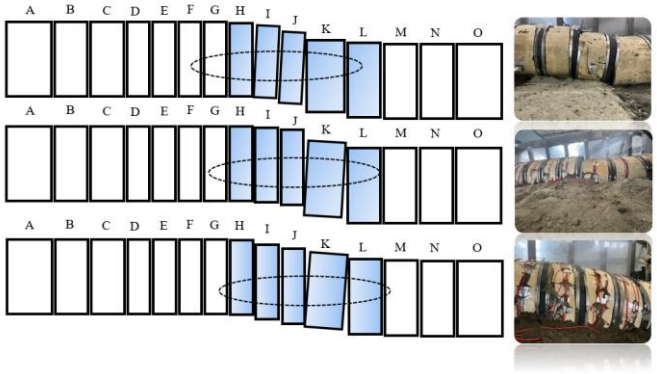

Fig. 8 Longitudinal deformation along the tunnel axis

To further analysis the typical tunnel longitudinal deformation in Figure 8, the absolute and relative displacements of the tunnel lining invert and crown with different fault dislocations detected by the internal tunnel displacement meters are given in Figure 9(a) and Figure 9(b) are the absolute displacement and convergence deformation curves of the structural vault and arch bottom distributed along the longitudinal direction of the tunnel under different displacement conditions respectively. Apparently, the absolute displacements of the tunnel invert and crown arch increase simultaneously with the dislocation levels. With the increase of dislocation, the tunnel invert and crown located in hanging wall have different settlements. With the gradual increase of dislocation, the relative displacement of the tunnel invert and the crown located in section J gradually increased, but the growth rate seems to be decreasing. The maximum relative displacement is 25 mm, at which the tunnel radial compression deformation is more significant.

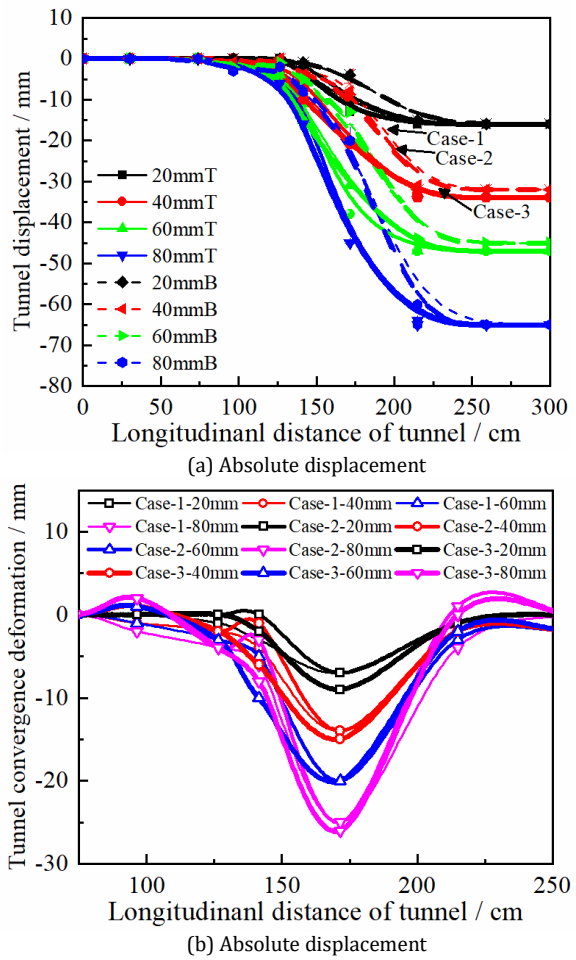

Fig. 9 Absolute and relative displacement of arch invert and crown

4.2 Transverse failure patterns

When the fault dislocation occurs, the tunnel will have a large overall deformation in the longitudinal direction, and it will also cause damage to the local part of structure. The damage is usually manifested as lining crack propagation and local falling of blocks. Figure 10 shows the actual damages of the most severely damaged sections of H, I, J or K in the three test cases.

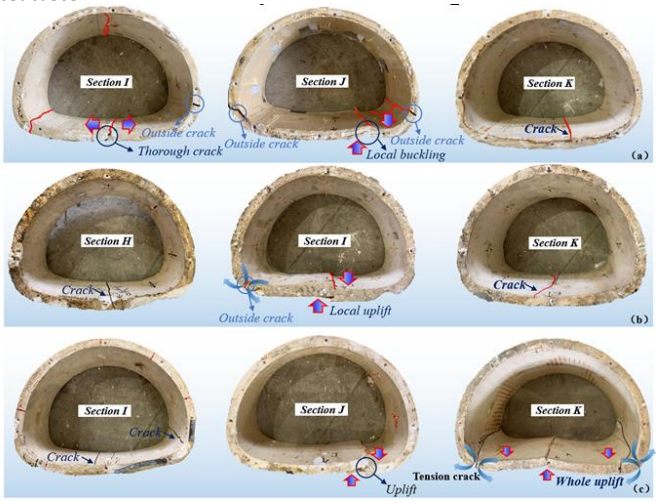

Fig. 10 Typical deformation and failure of sectional tunnel linings (a) Case-1; (b) Case-2; (c) Case-3

What can be seen from Figure 10 is that the uplift of inverted arch and the extension of tensioned cracks at arch feet are main characteristics in tunnel damage. It is noteworthy that the damage locations of lining are not concentrated in same sections in the three test cases. The most severely damaged sections are located at section J, I and K. This difference may be caused owing to the inconsistency of the fault parameters.

Based on the above test results, the damage types can be roughly classified into three types according to the degree of damage. First type is the penetrating cracks along the longitudinal tunnel on inverted arch such as the segments K (C1), H, K (C2) and I (C3). This damage type is attributed to the resistance of the inverted arch to the soil during the overall

downward movement of hanging wall, which results in a large tensile effect inside arch crown and the inverted arch. The unloading effect of the arch structure keeps it in a safer state. Therefore, longitudinal cracks appear and penetrate the position of the inverted arch. For convenience, this damage type is defined as Type 1, which is slight damage. Type 2 refers to that the section shape is gradually changed from a horseshoe shape to an oval shape on deformation. The failure behave is manifested as longitudinal cracks in the inverted arch, arch crown or arch foot. The representative segment is section I (C1, C2). The degree of damage is considered moderate damage. Finally, when the inverted arch has serious buckling, the floor will produce partial or total uplift. In this case, compression deformation is the most serious, and several cracks will appear. This damage type is concepted as Type 3, which is serious damage. The typical failure states of Type 3 are shown in J (C1), I (C2), J and K (C3). Obviously, the existence of faults will seriously affect the safety performance of tunnels. The tunnel is more susceptible to fault fracture zone.

5. Conclusions

Through large-scale model tests, the deformation and rupture features of ground surface and the deformation characteristic of tunnel under normal faulting were investigated and the safety performance of fault-crossing tunnel is examined. Results are obtained from the study as follows:

1. Under different dislocation momentum conditions, there is always an intersection point in surface deformation. The intersection points appear at 812 mm, 855 mm and 1125 mm, respectively. It can be seen that with the increase of fault dip angle, the position of this intersection gradually moves to the side of the active plate, and the smaller the fault dip angle, the more significant the intersection.
2. The surface deformation can be divided into four subregions, named stability region in footwall (Rs in footwall), coordination region (Rc), severe deformation region (Rsd in footwall), and stability region in hanging wall (Rs in hanging wall). As the fault dip angle increases, the severe deformation region (Rsd) gradually narrows. Coordination region (Rc) did not change significantly.
3. The tunnel near fault fracture zone will be the most seriously damaged part. Elliptical horseshoe shape is presented in transverse deformation subjected to normal faulting. Typical damage types can be divided into four categories according to the degree of damage: Type 0 (no damage), Type 1 (slight damage), Type 2 (moderate damage) and Type 3 (severe damage) respectively. In tunnel engineering, moderate damage or serious damage should be avoided as far as possible to guarantee the normal operation of the tunnel.

Credit author statement

Zhiyong Liu: Conceptualization, Methodology, Writing-original draft, Writing-review & Editing. Lingyin Zhao: Methodology, Conceptualization, Supervision, Writing-review & Editing. Dan Zhang: Data curation, Writing-review & Editing. Cheng Gong: Data curation, Writing-review & Editing. Ping Geng: Methodology, Conceptualization, Supervision, Data curation, Writing-review & Editing. Tianqiang Wang: Writing-review & Editing.

Conflict of interest

The authors declare that they have no known competing financial interests or personal relationships that could have appeared to influence the work reported in this paper.

Acknowledgement and supplementary data

The authors are grateful to anonymous reviewers for their valuable and most helpful comments.

Reference

Hashimoto M, Sagiya T, Tsuji H, et al. Co-seismic displacements of the 1995 Hyogo-ken Nanbu Earthquake[J]. Journal of Physics of the Earth, 1996, 44(4): 255-279. https://doi.org/10.4294/jpe1952.44.255

Zhou Q, Xu X, Yu G, et al. Width Distribution of the Surface Ruptures Associated with the Wenchuan Earthquake: Implication for the Setback Zone of the Seismogenic Faults in Postquake ReconstructionWidth Distribution of the Surface Ruptures: Implication for the Setback Zone of Seismogenic Faults[J]. Bulletin of the Seismological Society of America, 2010, 100(5B): 2660-2668. https://doi.org/10.1785/0120090293

Li H, Li X, Liu H. Deformation and failure mechanism of metro shield tunnel subjected to buried fault dislocation[J]. Engineering Failure Analysis, 2023, 153: 107551. https://doi.org/10.1016/j.engfailanal.2023.107551

Bao L, Wei F. Study on the response of tunnel lining under fault dislocation[J]. Sustainability, 2023, 15(6): 5150. https://doi.org/10.3390/su15065150

Scholz, C H. The mechanics of earthquakes and faulting [M]. Cambridge university press, 2019. https://doi.org/10.1017/9781316681473

Xu X W, Yu G H, Chen G H, et al. Analysis on the characteristics of near-surface geological deformation zones in the large strike-slip fault zone in the northern Qinghai-Tibet Plateau [J]. Earthquake Geology, 2007, (2): 201-217. （in Chinese）

Dai S H, Ma S L, Pan Y S, et al. Experimental study on rupture and propagation characteristics of hidden thrust faults and its seismic geological significance [J]. Earthquake Geology, 2008, 30(4): 945-956. (in Chinese)

Bo J S, Huang J Y, and Zhang J Y. A prediction method of surface rupture in strong earthquakes based on logistic regression analysis [J]. Earthquake Engineering and Engineering Dynamic, 2019, 39(4): 1-7.

Shen, C., Bo, J., Qi, W., Zhang, X., Huang, J., & Qiao, F. (2020). Analysis of the surface rupture process of strong earthquakes based on centrifuge tests. Soil Dynamics and Earthquake Engineering, 136, 106239. https://doi.org/10.1016/j.soildyn.2020.106239

Lin M L, Chung C F, Jeng F S, et al. The deformation of overburden soil induced by thrust faulting and its impact on underground tunnels [J]. Engineering Geology, 2007, 92(3-4): 110-132. https://doi.org/10.1016/j.enggeo.2007.03.008

Wang T Q, Geng P, Li P S, et al. Deformation and failure of overburden soil subjected to normal fault dislocation and its impact on tunnel [J]. Engineering Failure Analysis, 2022, 142: 106747. https://doi.org/10.1016/j.engfailanal.2022.106747

Han X M and Li W J. Numerical Analysis on the Structure Type and Mechanical Response of Tunnel Crossing Active Reverse Fault [J]. Geofluids, 2021, 2021. https://doi.org/10.1155/2021/5513042

Kiani M, Akhlaghi T, and Ghalandarzadeh A. Experimental modeling of segmental shallow tunnels in alluvial affected by normal faults [J]. Tunnelling and Underground Space Technology, 2016, 51: 108-119. https://doi.org/10.1016/j.tust.2015.10.005

Liu X Z, Li X F, Sang Y L, et al. Experimental study on normal fault rupture propagation in loose strata and its impact on mountain tunnels [J]. Tunnelling and Underground Space Technology, 2015, 49: 417-425. https://doi.org/10.1016/j.tust.2015.05.010

Disclaimer